Neuronal NPR-15 modulates molecular and behavioral immune responses via the amphid sensory neuron-intestinal axis in *C. elegans*

Benson Otarigho[1], Anna Frances Butts[1], and Alejandro Aballay[1,2,*]

[1]Department of Genetics, The University of Texas MD Anderson Cancer Center, Houston, TX

[2]Department of Microbiology and Molecular Genetics, McGovern Medical School at UTHealth Houston, TX

[3]Lead contact

[*]Correspondence: aaballay@mdanderson.org

Abstract

The survival of hosts during infections relies on their ability to mount effective molecular and behavioral immune responses. Despite extensive research on these defense strategies in various species, including the model organism *Caenorhabditis elegans*, the neural mechanisms underlying their interaction remain poorly understood. Previous studies have highlighted the role of neural G protein-coupled receptors (GPCRs) in regulating both immunity and pathogen avoidance, which is particularly dependent on aerotaxis. To address this knowledge gap, we conducted a screen of mutants in neuropeptide receptor family genes. We found that loss-of-function mutations in *npr-15* activated immunity while suppressing pathogen avoidance behavior. Through further analysis, NPR-15 was found to regulate immunity by modulating the activity of key transcription factors, namely GATA/ELT-2 and TFEB/HLH-30. Surprisingly, the lack of pathogen avoidance of *npr-15* mutant animals was not influenced by oxygen levels. Moreover, our studies revealed that the amphid sensory neuron ASJ is involved in mediating the immune and behavioral responses orchestrated by NPR-15. Additionally, NPR-15 was found to regulate avoidance behavior via the TRPM gene, GON-2, which may sense the intestinal distension caused by bacterial colonization to elicit pathogen avoidance. Our study contributes to a broader understanding of host defense strategies and mechanisms underlining the interaction between molecular and behavioral immune responses.

Keywords. G-protein-coupled receptors; immunity; avoidance behavior; and neuropeptides.

Introduction

Hosts employ multiple defense mechanisms to combat infections, including molecular immune defenses (1-3) and behavioral defense responses to invading pathogens (4-6). Overall, these strategies are conserved across species (5-8), but their relationship and mechanistic interplay are not yet fully elucidated. While the immunological defense response is effective, it is metabolically costly and may lead to inflammatory damage (9-12). On the other hand, the avoidance behavioral response serves as a crucial first line of defense, enabling hosts to prevent or minimize contact with pathogens (13-15). Although both immune and behavioral responses to pathogen infection are well documented in *Caenorhabditis elegans* (16-20), the relationship between these survival strategies remains poorly understood.

C. elegans is a valuable model organism for studying the genetic mechanisms that control host immune and behavioral responses to pathogens (21, 22). Although *C. elegans* lacks adaptive immunity, part of its innate immune response comprises evolutionarily conserved pathways and immune effectors (22). *C. elegans* has been widely used in research studies to investigate these pathways due to its well-defined nervous system and genetic tractability, making it an ideal model organism to explore pathways that are critical to immunity and avoidance behavior (23-25). Notably, intestinal changes triggered by bacterial pathogen colonization activate the DAF-7/TGF-β pathway and the G-protein coupled receptor (GPCR) NPR-1 pathway, which also regulates aerotaxis behavior (15, 16, 19, 26).

To uncover mechanisms that control immune and behavioral responses to invading pathogens independently of aerotaxis, we focused on studying mutants in *npr* genes that have not been previously linked to either host strategy against pathogen infection. Our investigation revealed that loss-of-function mutations in the NPR-15 encoding genes enhanced pathogen resistance when infected by Gram-negative and Gram-positive bacterial pathogens. Intriguingly, *npr-15* mutants exhibited a lack of pathogen avoidance behavior that was found to be independent of oxygen sensation. These findings point towards the involvement of a novel mechanism in the regulation of immune response and avoidance behavior.

Further analysis unveiled that the resistance to pathogen infection in *npr-15* mutants is mediated by the transcription factors GATA/ELT-2 and TFEB/HLH-30. These evolutionarily conserved transcription factors play vital roles in regulating immunity in *C. elegans* (27-31). Additionally, we discovered that NPR-15 controls avoidance behavior through the intestinal-expressed transient receptor potential melastatin (TRPM) ion channel, GON-2, which has recently been demonstrated to modulate avoidance behavior in Gram-positive bacteria (32). Moreover, our results indicate that the amphid sensory neuron, ASJ, plays a crucial role in the interplay between immune response and avoidance behavior. These findings provide insights into the neural mechanisms that control immunity against bacterial infections and pathogen avoidance behavior.

Results

NPR-15 loss-of-function enhances pathogen resistance and inhibits avoidance behavior independently of aerotaxis.

Out of 34 mutants in *npr* genes that were not previously linked to the control immunity (Table S1A), only animals lacking NPR-15 [*npr-15(tm12539)* and *npr-15(ok1626)* null animals] exhibited enhanced survival against *Pseudomonas aeruginosa*-mediated killing compared to wild-type (WT) animals (Figure 1A, S1A and Table S1B). Furthermore, we found that the *npr-15(tm12539)* animals exhibited less visible bacterial colonization and significantly reduced colony-forming units compared to WT animals (Figure 1B-C). The enhanced resistance to pathogen of *npr-15(ok1626)* animals appears to be universal, as the mutants were also found to be resistant to additional human pathogens, including Gram-negative *Salmonella enterica* strain 1344 and Gram-positive *Enterococcus faecalis* strain OG1RF and *Staphylococcus aureus* strain NCTCB325 (Figure 1D-F), suggesting that NPR-15 suppresses defense against bacterial pathogens in general. When exposed to live *Escherichia coli*, the primary food source of *C. elegans* in the laboratory, *npr-15(tm12539)* animals exhibited increased lifespan compared to WT animals (Figure 1G). However, there were no significant differences in longevity between *npr-15(tm12539)* and WT animals when they were exposed to lawns of *E. coli* that were rendered non-proliferating by ultraviolet light (UV) treatment (33) (Figure 1H). Expression of *npr-15* under the control of its own promoter rescued the enhanced survival of *npr-15(tm12539)* animals to different bacterial pathogens (Figures 1A-G), indicating that the functional loss of NPR-15 enhanced the animal's survival against live bacteria.

Considering that *C. elegans* exhibits avoidance behavior when encountering certain pathogenic bacteria (15, 17-19), we examined the lawn occupancy of *npr-15(tm12539)* and WT animals on the partial lawn of *S. aureus* cultured in the center of an agar plate (Figure 1I). Unexpectedly, we found that *npr-15(tm12539)* exhibited significantly reduced pathogen avoidance when exposed to *S. aureus* (Figure 1J). We also compared the re-occupancy of the lawn exhibited by WT and *npr-15(tm12539)* animals and found no differences in their re-occupancy (Figure S1B). Interestingly, we noticed that the variation in lawn occupancy is greater in WT than in *npr-15(tm12539)* animals across experiments (Table S2), which suggests that the strong lack of avoidance of *npr-15(tm12539)* somehow counteracts the experimental variation. We also found that *npr-15(tm12539)* exhibited reduced learned avoidance compared to WT animals (Figure S1C).

To investigate whether aerotaxis played a role in the lack of avoidance of *S. aureus* exhibited by *npr-15(tm12539)*, we studied lawn occupancy in the presence of 8% oxygen. As shown in Figure S1D, exposure to 8% oxygen to *npr-15(tm12539)* animals did not rescue the lack of avoidance to *S. aureus*, although it did rescue the lack of avoidance of *npr-1* mutants. Moreover, the survival of *npr-15(tm12539)* animals on full-lawn assays, where agar plates were completely covered by pathogenic bacteria to eliminate the possibility of pathogen avoidance, was significantly higher than that of WT animals (Figure S1E-F). These findings suggest that NPR-15 suppresses pathogen resistance and enhances avoidance behavior in response to pathogen infection, independently of oxygen concentrations.

Because *C. elegans* pharyngeal pumping directly affects bacterial intake (16, 19, 34, 35), we asked whether the resistance to infections and reduced pathogen avoidance behavior in *npr-15(tm12539)* animals could be attributed to a decrease in pathogen intake. We found that *npr-15(tm12539)* animals exhibited pumping rates comparable to that of WT animals (Figure S1G), indicating that the dose of pathogens is similar in both cases. Moreover, it has recently been demonstrated that bacterial accumulation in animals defective in the defecation motor program (DMP) causes intestinal distension that elicits a robust immune response (19) and modulates pathogen avoidance (19, 26, 32, 36, 37). However, we found that the defecation cycle of *npr-*

15(tm12539) animals is indistinguishable from that of WT animals (Figure S1H). Taken together, our results show that NPR-15 loss-of-function enhances pathogen resistance and inhibits avoidance behavior, suggesting NPR-15 suppresses molecular immunity while activating behavioral immunity.

The loss of NPR-15 leads to the upregulated immune and neuropeptide genes.

To understand the immune mechanisms controlled by NPR-15 in defense against pathogen exposure, we conducted transcriptomic analyses to identify dysregulated genes in *npr-15(tm12539)* compared to WT animals (Figure 2A and Table S3). To identify gene groups that were controlled by NPR-15, we performed an unbiased gene enrichment analysis using a WormBase enrichment analysis tool (https://wormbase.org/tools/enrichment/tea/tea.cgi) that is specific for *C. elegans* gene data analyses (38). The study revealed 10 ontology clusters with high enrichment scores of vital biological functions for upregulated and downregulated genes in *npr-15(tm12539)* (Figure 2B, S2). Overall, the gene expression data showed significant upregulation of immune/defense response and neuropeptide signaling pathway genes (Figure 2B). Genes associated with synaptic signaling, ligand-gated channel activity, lipid metabolism, and response to biotic stimuli were also upregulated in *npr-15(tm12539)* animals.

To further explore potential immune pathways involved in pathogen resistance in NPR-15-deficient animals, we performed a gene enrichment analysis using the immune gene subset with the Worm Exp tool (https://wormexp.zoologie.uni-kiel.de/wormexp/) (39). This tool integrates all published expression datasets for *C. elegans* to analyze and generate pathways. Our analysis revealed a high enrichment of pathways crucial for *C. elegans* defense against bacterial infections, including the ELT-2, HLH-30, PMK-1, and DAF-2/DAF-16 insulin pathways (Figure 2C and Table S4) (28, 30, 31, 40-45). Notably, we observed that several of the PMK-1, HLH-30, and DAF-16-dependent genes were also controlled by ELT-2 (Figure 2D), suggesting a potentially major role of ELT-2-dependent genes in the enhanced resistance to the pathogen phenotype of *npr-15(tm12539)* animals. To validate these findings, we performed Quantitative PCR (qPCR) and confirmed the upregulation of ELT-2-dependent immune genes such as *dct-17*, C29F3.7, T19D12.4, C32H11.4, C34H4.1 and *clec-86* (Figure 2E). We also validated HLH-30-

dependent genes T21F4.1, *argn-1*, F53A9.8, and *pnp-1* (Figure 2F). These transcriptomic and gene analyses indicate that NPR-15 primarily regulates *C. elegans* defense against bacterial infections by inhibiting immune genes, several of which are controlled by ELT-2, HLH-30, and PMK-1.

NPR-15 controls ELT-2 and HLH-30-dependent genes via sensory neuron, ASJ.

To investigate whether the enhanced resistance to pathogen infection of *npr-15(tm12539)* animals is due to the upregulation of immune genes, we examined the role of RNA interference (RNAi)-mediated suppression of the immune pathways shown in Figure 2C. We inactivated *elt-2, pmk-1, hlh-30,* and *daf-16* in WT and *npr-15(tm12539)* animals and exposed them to *S. aureus*. We found that *elt-2* RNAi completely suppressed the enhanced resistance to *S. aureus* infection in *npr-15(tm12539)* animals (Figure 3A). Partial suppression of pathogen resistance in *npr-15(tm12539)* animals was observed with *hlh-30* RNAi (Figure 3B). Furthermore, when both *hlh-30* and *elt-2* were inactivated in *npr-15(tm12539)* animals and were exposed to *S. aureus*, their susceptibility to infection was comparable to that of *elt-2* RNAi animals (Figure 3C). However, *pmk-1*, *daf-16* RNAi failed to suppress the pathogen resistance of *npr-15(tm12539)* (Figure 3D-E). To confirm these findings, we crossed mutants in the aforementioned immune regulators to *npr-15(tm12539)* animals and exposed them to *S. aureus* (Figure S3A-C). We also studied the aforementioned immune pathways in the response of *npr-15(tm12539)* animals to *P. aeruginosa* (Figure S3D-F). We found that *hlh-30* or *pmk-1* mutation partly suppressed the resistance to *P. aeruginosa* infection phenotype of *npr-15(tm12539)* animals (Figure S3D and E). These results indicate that NPR-15 suppresses ELT-2 and HLH-30-dependent molecular immunity.

Because NPR-15 is expressed in six sensory neuronal cells (ASG, ASI, ASJ, ASE, AFD, and AWC) as well as an interneuron, AVK (Figure 4A) (46), we studied whether the NPR-15-expressing cells could control the defense response against pathogen infection. Firstly, we examined the neuronal connectome and communication between the NPR-15-expressing cell and found well-established synaptic connections between all the sensory neurons (Figure 4A). Next, we asked if NPR-15 could be acting in a neuron-intrinsic manner to control immune response. To address this question, we specifically inactivated *npr*-15 in neurons and the intestine using

tissue-specific RNAi strains and assessed the survival of the animals after *S. aureus* infection. Unlike intestine-specific RNAi (strain MGH171) (Figure S4A), neural-specific RNAi (strain TU3401) of NPR-15 resulted in a pathogen resistance phenotype similar to that of *npr-15(tm12539)* animals (Figure S4B). This finding was further supported by rescuing NPR-15 under the control of a pan-neuronal promoter and exposing the animals to *S. aureus*. The results demonstrated that pan-neuronal promoter-driven expression of NPR-15 rescued the enhanced survival phenotype of *npr-15(tm12539)* animals (Figure 4B). These results suggest that NPR-15 suppresses immunity through the nervous system. We next studied the specific NPR-15-expressing neuronal cells (ASG, ASI, ASJ, ASE, AFD, AWC) that could control the defense response against pathogen infection. To identify the neuronal cells responsible for the NPR-15-mediated immune control, we crossed strains lacking the neurons with *npr-15(tm12539)* animals and studied their effect on defense against pathogen infection (Figure 4C-E and S4C-E). We found that ASJ(-) animals exhibited resistance to pathogen-mediated killing similar to that of *npr-15(tm12539)* animals (Figure 4C). Although the ASG(-) and ASE(-) neuron-ablated strains demonstrated pathogen resistance phenotype, there is a significant difference compared to that of *npr-15(tm12539)* animals (Figure 4D-E). Hence, we further confirmed the role of NPR-15/ASJ neurons in suppressing immunity by rescuing NPR-15 on ASJ unique promoter and performing survival experiments with the rescued strain. Results showed that the ASJ-specific rescue of NPR-15 successfully blocked the enhanced survival of *npr-15(tm12539)* animals (Figure 4F). We also quantified the expression of immune genes and found that they were upregulated in ASJ(-) animals (Figure 4G). Collectively, these findings suggest that NPR-15 controls immunity in a manner similar to that of ASJ neurons.

The lack of avoidance behavior by NPR-15 loss-of-function is independent of immunity and neuropeptide genes.

Having established the upregulation of immune genes in *npr-15(tm12539)* animals compared to WT animals (Figure 2B-F and Table S4), we determine whether the reduced pathogen avoidance of *npr-15(tm12539)* animals could be attributed to the upregulation of immune pathways. To investigate this, we employed RNAi to suppress immune transcription factors/regulators and evaluated their impact on pathogen avoidance behavior in both WT and *npr-15(tm12539)* animals. Our results indicate that none of the tested immune regulators (*elt-2, pmk-1, daf-16,* and

hlh-30) were able to suppress the lack of pathogen avoidance behavior observed in response to *S. aureus* (Figure S5A-D). Furthermore, we inactivated immune genes that are not controlled by the immune regulators tested above, but none of them were able to suppress the lack of avoidance behavior in the *npr-15(tm12539*) animals (Table S5). Given the possibility of functional redundancy among these genes, we cannot rule out the possibility that different combinations may play a role in controlling avoidance behavior. These findings indicate that the avoidance behavior observed in *npr-15(tm12539)* is independent of individual immune genes upregulated in *npr-15(tm12539*) animals.

Additionally, previous studies have shown that neuropeptides expressed in the intestine can modulate avoidance behavior (47), and we found that neuropeptides are among the most highly upregulated genes in *npr-15(tm12539)* animals (Figure 2B and Table S6). To study whether an intestinal signal may act through NPR-15 to regulate avoidance, we inactivated the upregulated intestinal neuropeptide genes in *npr-15(tm12539)* animals. Our experiments revealed that none of the inactivated intestinal-expressed neuropeptides were able to suppress the lack of avoidance behavior of *npr-15(tm12539)* animals in response to *S. aureus* (Figure S5E and Table S5). Therefore, it can be concluded that the absence of avoidance behavior by loss of NPR-15 function is independent of both immune and intestinal neuropeptide signaling pathways.

NPR-15 controls pathogen avoidance via sensory neuron, ASJ, and intestinal TRPM channel, GON-2.

Having demonstrated that NPR-15 controls immune response via sensory neurons, ASJ (Figure 4C, 4F-G), we sought to identify the neurons involved in the lack of avoidance behavior to *S. aureus* observed in *npr-15(tm12539)* animals. First, we investigated the avoidance behavior of a pan-neuronal rescued strain of NPR-15, which successfully rescued the suppressed pathogen avoidance of *npr-15(tm12539)* animal (Figure 5A). Next, we asked which of the NPR-15-expressing-neuronal cells could control pathogen avoidance. To answer this question, we evaluated the pathogen avoidance of the different neuron-ablated strains that were crossed with *npr-15(tm12539)* animals. Consistent with our previous findings, we found that only ASJ(-) exhibited reduced pathogen avoidance similar to that of *npr-15(tm12539)* animals (Figure 5B). This observation was further confirmed by rescuing NPR-15 under the control of an ASJ unique

promoter (Figure 5C). The pathogen avoidance of other neuronal-ablated strains was comparable to that of WT animals (Figure 5D-G). These results suggest that the loss of NPR-15 function suppresses behavioral immunity via sensory neurons, specifically ASJ.

Because transient receptor potential melastatin (TRPM) ion channels, GON-2 and GTL-2, are required for pathogen avoidance (32), we studied whether they may be part of the NPR-15 pathway that controls pathogen avoidance. We inactivated *gon-2* and *gtl-2* in *npr-15(tm12539)* animals and WT animals. Our findings showed that only *gon-2* null animals, but not *gtl-2*, exhibited pathogen avoidance behavior similar to that of *npr-15(tm12539)* animals (Figure 5H-I). This suggests that both NPR-15 and GON-2 may function in a shared pathway to regulated pathogen avoidance behavior. As it has been previously demonstrated that GON-2 modulates avoidance behavior through the intestine (32), we confirmed the role of intestinal-expressed GON-2 in pathogen avoidance by inactivating *gon-2* in an RNAi intestine-specific strain (MGH171), as well as in an RNAi neuron-specific strain TU3401) that was used as a control. These animals were exposed to *S. aureus* to study their lawn occupancy. Our results showed that the inactivation of *gon-2* in MGH171 and MGH171;*npr-15(tm12539)* (Figure 5J), but not in TU3401 (Figure S6), exhibited comparable avoidance behaviors to that of *npr-15(tm12539)* animals. These results suggest that NPR-15 acts through the intestinal TRPM channel GON-2 to control pathogen avoidance behavior. Since we have previously shown that only ASJ(-) animals among other neuron-ablated strains exhibit a similar avoidance behavior to *npr-15(tm12539*) animals (Figure 5B, 5D-G), we investigated whether NPR-15 control of avoidance behavior towards *S. aureus* in a GON-2-dependent manner involves ASJ. We used RNAi to inactivate *gon-2* in ASJ(-), ASJ(-);*npr-15(tm152799)*, *npr-15(tm12539)*, and WT animals before exposing them to *S. aureus* to assay their lawn occupancy. Our results showed that the avoidance behavior of ASJ(-);*gon-2* is comparable to that of ASJ(-), ASJ(-);*npr-15(tm12539)*, and *gon-2* null animals when exposed to *S. aureus* (Figure 5K). These results suggest that NPR-15 controls *S. aureus* avoidance in a GON-2-dependent manner via the ASJ neuron. In summary, the neuronal GPCR/NPR-15 plays a dual role: suppressing the immune response and enhancing avoidance behavior towards *S. aureus* through sensory neurons, specifically ASJ. The control of immunity against the pathogen *S. aureus* is dependent on the ELT-2 and HLH-30 transcription factors,

while the control of avoidance behavior is GON-2-dependent and mediated through the intestine (Figure 6).

Discussion

GPCRs play a crucial role in neuronal and non-neuronal tissues in shaping both immune and avoidance behavioral responses toward invading pathogens (48). In this study, we investigated the dual functionality of GPCR/NPR-15 in regulating molecular innate immunity and pathogen avoidance behavior independently of aerotaxis. Additionally, we aimed to understand the mechanism by which the nervous system controls the interplay between these crucial survival strategies in response to pathogenic threats. Our findings indicate that NPR-15 suppresses immune responses against different pathogen infections by inhibiting the activity of the GATA/ELT-2 and HLH-30 immune transcription regulators. Moreover, we found that the control of the pathogen avoidance behavior by NPR-15 is independent of aerotaxis and dependent on intestinal GON-2. Furthermore, we demonstrated that NPR-15 controls the immunity-behavioral response via an amphid sensory neuron, ASJ, in response to *S. aureus* infection.

ASJ neurons are known to regulate different biological functions such as lifespan (49), dauer activities (50, 51), head-directed light avoidance (52), and food search (53). We show here that ASJ neurons play a role in the control of immune and behavioral responses against pathogen infection through GPCR/NPR-15. Our research additionally indicates that the regulation of NPR-15-mediated avoidance is not influenced by intestinal immune and neuropeptide genes. Given the potential for functional redundancy and our focus on genes upregulated in the absence of NPR-15, we cannot entirely rule out the possibility that unexamined immune effectors or neuropeptides, not transcriptionally controlled by NPR-15, might be involved. Different intestinal signals may also participate in the NPR-15 pathway that controls pathogen avoidance.

Other neural GPCRs have also been linked to the control of innate immunity in *C. elegans* (16, 54, 55). For example, the octopamine receptor OCTR-1 (20), the olfactory learning receptor OLRN-1 (56), and the D1-like dopamine receptor DOP-4 (57) function in ASH/ASI, AWC, and ASG neurons, respectively. GPCRs that are neuropeptide receptors, such as NPR-1 (16), NPR-9 (58), and NPR-8 (35), also function in neurons to control immunity. In common, these GPCRs regulate innate immunity via the p38/PMK-1 MAPK pathway (16, 34, 35, 56-58).

In contrast, NPR-15 functions in ASJ neurons to suppress immune defense against bacterial infections by inhibiting the transcriptional activity of ELT-2 and HLH-30. Two of these GPCRs, NPR-1 (16) and PCDR-1 (59), also play a role in mediating pathogen avoidance. While OCTR-1-expressing neurons ASI play a role in avoidance (34), the specific role of OCTR-1 in ASH and ASI neurons remains unclear.

Our findings shed light on the role of NPR-15 in the control of the immune response. NPR-15 seems to suppress specific immune genes while activating pathogen avoidance behavior to minimize potential tissue damage and the metabolic energy cost associated with activating the molecular immune response against pathogen infections. Overall, the control of immune activation is essential for maintaining homeostasis and preventing excessive tissue damage caused by an overly aggressive and energy-costly response against pathogens (60-63).

Conclusion

Our research uncovers the dual regulatory role of NPR-15 in both immunity and avoidance behavior, independent of aerotaxis, mediated by amphid sensory neurons. The host relies on behavioral responses to minimize or completely avoid pathogen exposure, effectively preventing the activation of the immune pathways and production of immune effector molecules, which can be metabolically costly. Moreover, the sustained and prolonged activation of the molecular immune system can have detrimental effects on the host. Understanding the organismal control of molecular and behavioral immune responses to pathogens can provide valuable insights into universal mechanisms used across species to maintain homeostasis during infections.

Materials and Methods

Bacterial strains

The bacterial strains used in this study are *Escherichia coli* OP50, *E. coli* HT115(DE3) (64), *Pseudomonas aeruginosa* PA14, *P. aeruginosa* PA14-GFP (65, 66), *Salmonella enterica* Serovar Typhimurium 1344 (67), and *Staphylococcus aureus* strain NCTCB325 (68). Gram-negative bacteria were grown in Luria-Bertani (LB) broth. *Staphylococcus aureus* strain NCTCB325 was grown in Tryptic Soy Agar prepared with nalidixic acid. All bacteria were grown at 37°C.

***C. elegans* Strains and Growth Conditions**

Hermaphrodite *C. elegans* (var. Bristol) Wild-type (WT) was used as control unless otherwise indicated. *C. elegans* strains RB1429 *npr-15(ok1626)*, CX14394 *npr-5(ok1583)*, RB1836 *npr-14(ok2375)*, RB1289 *npr-18(ok1388)*, RB1405 *npr-22(ok1598)*, VC2526 *npr-35(ok3258)*, DA609 *npr-1(ad609)*, IM222 *npr-1(ur89)*, CX4148 *npr-1(ky13)*, CZ9957 *gtl-2(n2618)*, EJ1158 *gon-2(q388)*, EJ26 *gon-2(q362)*, LH202 *gtl-2(tm1463)*, JIN1375 *hlh-30(tm1978)*, CF1038 *daf-16(mu86)*, KU25 *pmk-1(km25)*, RB1668 *C02H7.2(ok2068)*, RB1632 *T02E9.1(ok2008)*, VC2421 *R106.2(ok3192)*, PS8315 *npr-29(sy1270)*, RB1365 *npr-16(ok1541)*, RB1958 *T07D4.1(ok2575)*, PS8484 *npr-31(sy1360)*, RB1429 *npr-15(ok1626)*, RB1325 *C53C7.1(ok1442)*, RB1938 *Y116A8B.5(ok2541)*, PS8177 *npr-23(sy1203)*, PS8317 *npr-33(sy1272)*, PS8450 *npr-27(sy1315)*, PS8444 *npr-21(sy1309)*, PS8442 *npr-26(sy1307)*, CX14394 *npr-5(ok1583)*, RB1836 *W05B5.2(ok2375)*, RB1405 *Y59H11AL.1(ok1598)*, MGH171 *alxIs9* [*vha-6p::sid-1::SL2::GFP*], TU3401 *uIs69* [*pCFJ90 (myo-2p::mCherry) + unc-119p::sid-1*], DA609 *npr-1(ad609)*, DA508 *npr-1(n1353)*, GR2245 *skn-1(mg570)*, JPS582 *vxEx582 [gcy-8p::ICE + myo-2p::mCherry] [AFD(-)]*, *PR680 che-1(p680)* [ASE(-)], PR674 *che-1(p674)* [ASE(-)], PR672 *che-1(p672)* [ASE(-)], JN1713 *peIs1713 [sra-6p::mCasp-1 + unc-122p::mCherry]* [ASH(-)], KJ412 *trx-1(jh127)* [ASJ(-)], *VZ1 trx-1(ok1449)* [ASJ(-)], RB1332 *trx-1(ok1449)* [ASJ(-)], JN1715 *peIs1715 [str-1p::mCasp-1 + unc-122p::GFP]* [AWB(-)], PS6025 *qrIs2 [sra-9::mCasp1]* [ASK(-)], and PY7505 *oyIs84 [gpa-4p::TU#813 + gcy-27p::TU#814 + gcy-27p::GFP + unc-122p::DsRed]* [ASI(-)] were obtained from the Caenorhabditis Genetics Center (University of Minnesota, Minneapolis, MN). We also obtained FX22538 *npr-15(tm12539)*, FX21950 *npr-3(tm1583)*, FX01583 *npr-3(tm11950)*, FX01782 *npr-4(tm1782)*, FX01497 *npr-6(tm1497)*, FX01498 *npr-12(tm1498)* and FX01504 *npr-13(tm1504)*, FX01665 *npr-34(tm1665)*, FX31809 *npr-30(tm6617)*, FX21079 *npr-28(tm1155)*, FX22538 *npr-15(tm12539)*, FX21950 *npr-3(tm11950)*, FX01583 *npr-3(tm1583)*, FX01782 *npr-4(tm1782)*, FX01497 *npr-6(tm1497)*, FX01498 *npr-12(tm1498)*, FX01504 *npr-13(tm1504)*, FX03170 *npr-17(tm3170)*, FX03225 *npr-17(tm3225)*, FX03170 *npr-17(tm3170)*, FX03225 *npr-17(tm3225)*, FX31312 *npr-22(tm8953)* from National Bioresource Project (NBRP), Japan. ASE(-);*npr-15(tm12539)*, ASI(-);*npr-15(tm12539)*, ASJ(-);*npr-15(tm12539)*, ASG(-);*npr-15(tm12539)*, *daf-16(mu86); npr-15(tm12539)*, *pmk-1(km25);npr-15(tm12539)*, *hlh-30(tm1978);npr-15(tm12539)*, *skn-1(mg570);npr-15(tm12539)* and ASG(-):*npr-15(tm12539)* were obtained by standard genetic

crosses. Rescued strain *npr-15(tm12539);Pnpr-15::npr-15*, neuronal rescued strain *npr-15(tm12539);Prab-3::npr-15* and *npr-15* rescued in ASJ neuron-specific, *npr-15(tm12539);Ptrx-1::npr-15*were generated as described below. The ASG(-) ablated Ex[*Ptax-2::*CZ*::ced-3(p17)::unc-54* 3'UTR + *Plim-6::ced-3(p15)*-NZ*::unc-54* 3'UTR, pRF4] was generated from our previous project (61). The strains were crossed with the WT laboratory N2. All strains were grown at 20°C on nematode growth medium (NGM) plates seeded with *E. coli* OP50 as the food source (69) unless otherwise indicated. The recipe for the control NGM plates is: 3 g/l NaCl, 3 g/l peptone, 20 g/l agar, 5 μg/ml cholesterol, 1 mM MgSO4, 1 mM CaCl2, and 25 mM potassium phosphate buffer (pH 6.0). The NGM plates were without antibiotics except as indicated.

RNA Interference (RNAi)

Knockdown of targeted genes was obtained using RNAi by feeding the animal with *E. coli* strain HT115(DE3) expressing double-stranded RNA (dsRNA) homologous to a target gene (70, 71). RNAi was carried out as described previously (20). Briefly, *E. coli* with the appropriate vectors were grown in LB broth containing ampicillin (100 μg/mL) and tetracycline (12.5 μg/mL) at 37°C overnight and plated onto NGM plates containing 100 μg/mL ampicillin and 3 mM isopropyl β-D-thiogalactoside (IPTG) (RNAi plates). RNAi-expressing bacteria were grown at 37°C for 12-14 hours. Gravid adults were transferred to RNAi-expressing bacterial lawns and allowed to lay eggs for 2-3 hours. The gravid adults were removed, and the eggs were allowed to develop at 20°C to young adults. This was repeated for another generation (except for ELT-2 RNAi) before the animals were used in the experiments. The RNAi clones were from the Ahringer RNAi library.

***C. elegans* Survival Assay on Bacterial Pathogens**

P. aeruginosa and *S. enterica* were incubated in LB medium. *S. aureus* was incubated in a TSA medium with nalidixic acid (20 μg/mL). The incubations were done at 37°C with gentle shaking for 12 hours. *P. aeruginosa* and *S. enterica* were grown on a modified NGM agar medium of 0.35% peptone and TSA respectively. For partial lawn assays, 20 μl of the overnight bacterial cultures were seeded at the center of the relevant agar plates without spreading. For full lawn experiments, 20 μl of the bacterial culture was seeded and spread all over the surface of the agar plate. No antibiotic was used for *P. aeruginosa* and *S. enterica*, while nalidixic acid (20 μg/mL)

was used for the TSA plates for *S. aureus*. The seeded plates were allowed to grow for 12 hours at 37°C. The plates were left at room temperature for at least 1 hour before the infection experiments. 20 synchronized young adult animals were transferred to the plates for infection, three technical replicate plates were set up for each condition (n = 60 animals) and the experiments were performed in triplicate. The plates were then incubated at 25°C. Scoring was performed every 12 hours for *P. aeruginosa* and *S. aureus*, and 24 hours for *S. enterica*. Animals were scored as dead if the animals did not respond to touch by a worm pick or lack of pharyngeal pumping. Live animals were transferred to fresh pathogen lawns each day. All *C. elegans* killing assays were performed three times independently.

Bacterial lawn avoidance assay

Bacterial lawn avoidance assays were performed by 20 mL of *P. aeruginosa* PA14 and *S. aureus* NCTCB325 on 3.5-cm modified NGM agar plates (0.35% peptone) and (0.35 % TSA) respectively, which were cultured at 37°C overnight to have a partial lawn. The modified NGM plates were left to cool to room temperature for about 1 hour, and 20 young adult animals grown on *E. coli* OP50 were transferred to the center of each bacterial lawn afterward. The number of animals on the bacterial lawns was counted at 12 and 24 hours after exposure.

Aversive training

Training plates of 3.5 cm diameter containing either *E. coli* OP50 on SK agar or *S. aureus* on TSA agar were prepared as described previously. Young gravid adult hermaphroditic animals that were grown on *E. coli* OP50 were washed with M9 and transferred to the training plates. They were allowed to roam for 4 hours at 25°C. After this, the animals were rewashed and transferred to a TSA plate containing lawn occupancy TSA-plated seed with *S. aureus*, as described above. The number of animals on the bacterial lawns was counted.

Avoidance assays at 8% oxygen

Avoidance assays as described above were carried out in a hypoxia chamber. Briefly, after young gravid adult hermaphroditic animals were transferred to the avoidance plates, the plates were placed in the hypoxia chamber and the lids of the plates were removed. The chamber was purged

with 8% oxygen (balanced with nitrogen) for 5 min at a flow rate of 25 L/min. The chamber was then sealed, and assays were carried out. Control plates were incubated at ambient oxygen.

Pharyngeal pumping rate assay

WT and *npr-15(tm12539)* animals were synchronized by placing 20 gravid adult worms on NGM plates seeded with *E. coli* OP50 and allowing them to lay eggs for 60 min at 20°C. The gravid adult worms were then removed, and the eggs were allowed to hatch and grow at 20°C until they reached the young adult stage. The synchronized worms were transferred to NGM plates fully seeded with *P. aeruginosa* for 24 hours at 25°C. Worms were observed under the microscope with a focus on the pharynx. The number of contractions of the pharyngeal bulb was counted over 60 s. Counting was conducted in triplicate and averaged to obtain pumping rates.

Defecation rate assay

WT and *npr-15(tm12539)* animals were synchronized by placing 20 gravid adult worms on NGM plates seeded with *E. coli* OP50 and allowing them to lay eggs for 60 min at 20°C. The gravid adult worms were then removed, and the eggs were allowed to hatch and grow at 20°C until they reached the young adult stage. The synchronized worms were transferred to NGM plates fully seeded with *P. aeruginosa* for 24 hours at 25°C. Worms were observed under a microscope at room temperature. For each worm, an average of 10 intervals between 2 defecation cycles were measured. The defecation cycle was identified as a peristaltic contraction beginning at the posterior body of the animal and propagating to the anterior part of the animal followed by feces expulsion.

Brood Size Assay

The brood size assay was done following the earlier described methods (72, 73). Ten L4 animals from egg-synchronized populations were transferred to individual NGM plates (seeded with *E. coli* OP50) (described above) and incubated at 20°C. The animals were transferred to fresh plates every 24 hours. The progenies were counted and removed every day.

C. elegans Longevity Assays

Longevity assays were performed on NGM plates containing live, UV-killed *E. coli* strains HT115 or OP50 as described earlier (20, 36, 61, 73). Animals were scored as alive, dead, or gone each day. Animals that failed to display touch-provoked or pharyngeal movement were scored as dead. Experimental groups contained 60 to 100 animals and the experiments were performed in triplicate. The assays were performed at 20°C.

Intestinal Bacterial Loads Visualization and Quantification

Intestinal bacterial loads were visualized and quantified as described earlier (20, 73). Briefly, *P. aeruginosa*-GFP lawns were prepared as described above. The plates were cooled to ambient temperature for at least an hour before seeding with young gravid adult hermaphroditic animals and the setup was placed at 25°C for 24 hours. The animals were transferred from *P. aeruginosa*-GFP plates to the center of fresh *E. coli* plates for 10 min to eliminate *P. aeruginosa*-GFP on their body. The step was repeated two times more to further eliminate external *P. aeruginosa*-GFP left from earlier steps. Subsequently, 10 animals were collected and used for fluorescence imaging to visualize the bacterial load while another 10 were transferred into 100 µL of PBS plus 0.01% Triton X-100 and ground. Serial dilutions of the lysates (10^1-10^{10}) were seeded onto LB plates containing 50 µg/mL of kanamycin to select for *P. aeruginosa*-GFP cells and grown overnight at 37°C. Single colonies were counted the next day and represented as the number of bacterial cells or CFU per animal.

Fluorescence Imaging

Fluorescence imaging was carried out as described previously (73). Briefly, animals were anesthetized using an M9 salt solution containing 50 mM sodium azide and mounted onto 2% agar pads. The animals were then visualized for bacterial load using a Leica M165 FC fluorescence stereomicroscope. The diameter of the intestinal lumen was measured using Fiji-ImageJ software. At least 10 animals were used for each condition.

RNA Sequencing and Bioinformatic Analyses

Approximately 40 gravid WT and *npr-15(tm12539)* animals were placed for 3 hours on 10-cm NGM plates (seeded with *E. coli* OP50) (described above) to have a synchronized population,

which developed and grew to L4 larval stage at 20°C. Animals were washed off the plates with M9 and frozen in QIAzol by ethanol/dry ice and stored at -80 prior to RNA extraction. Total RNA was extracted using the RNeasy Plus Universal Kit (Qiagen, Netherlands). Residual genomic DNA was removed using TURBO DNase (Life Technologies, Carlsbad, CA). A total of 6 µg of total RNA was reverse-transcribed with random primers using the High-Capacity cDNA Reverse Transcription Kit (Applied Biosystems, Foster City, CA).

The library construction and RNA sequencing in Illumina NovaSeq 6000 platform was done following the method described by (74) and (75) pair-end reads of 150 bp were obtained for subsequent data analysis. The RNA sequence data were analyzed using a workflow constructed for Galaxy (https://usegalaxy.org) as described (76) and was validated using Lasergene DNA star software. The RNA reads were aligned to the *C. elegans* genome (WS271) using the aligner STAR. Counts were normalized for sequencing depth and RNA composition across all samples. Differential gene expression analysis was then performed on normalized samples. Genes exhibiting at least two-fold change were considered differentially expressed. The differentially expressed genes were subjected SimpleMine tools from WormBase (https://www.wormbase.org/tools/mine/simplemine.cgi) to generate information such as WormBase ID and gene name, which are employed for further analyses. Gene ontology analysis was performed using the WormBase IDs in DAVID Bioinformatics Database (https://david.ncifcrf.gov) (77) and validated using a *C. elegans* data enrichment analysis tool (https://wormbase.org/tools/enrichment/tea/tea.cgi). The enrichment analysis tool on WormBase indicates that all significantly enriched terms have a Q value less than 0.1. Immune and age determination pathways were obtained using the Worm Exp version 1 (http://wormexp.zoologie.uni-kiel.de/wormexp/) (39) using the transcription factor target category. The Venn diagrams were obtained using the web tool InteractiVenn (http://www.interactivenn.net) (78) and bioinformatics and evolutionary genomics tool (http://bioinformatics.psb.ugent.be/webtools/Venn/). While neuron wiring was done using the database of synaptic connectivity of *C. elegans* for computation (79) http://ims.dse.ibaraki.ac.jp/ccep-tool/.

RNA Isolation and Quantitative Reverse Transcription-PCR (qRT-PCR)

Animals were synchronized and total RNA extraction was done following the protocol described above. qRT-PCR was conducted using the Applied Biosystems One-Step Real-time PCR protocol using SYBR Green fluorescence (Applied Biosystems) on an Applied Biosystems 7900HT real-time PCR machine in 96-well-plate format. Twenty-five microliter reactions were analyzed as outlined by the manufacturer (Applied Biosystems). The relative fold changes of the transcripts were calculated using the comparative $CT(2^{-\Delta\Delta CT})$ method and normalized to pan-actin (*act-1, -3, -4*). The cycle thresholds of the amplification were determined using StepOnePlus™ Real-Time PCR System Software v2.3 (Applied Biosystems). All samples were run in triplicate. The primer sequences were available upon request and presented in Table S7.

Generation of transgenic *C. elegans*

To generate *npr-15* rescue animals, the DNA *npr*-15 alongside its promoter was amplified from the genomic DNA of Bristol N2 *C. elegans* adult worms. Plasmid pPD95_77_*Pnpr-15_npr-15* was constructed by linearization of plasmid pPD95_77 using HindIII and SalI restriction digestion enzymes. The amplified *Pnpr-15::npr-15* DNA was cloned behind its native promoter in the plasmid pPD95_77, between HindIII and SalI sites. For the neuronal rescue strain, the plasmid pPD95_77_*Prab-3_npr-15* was constructed by cloning amplified *npr-15* DNA into BamHI/KpnI digested pPD95_77_*Prab-3* under the promoter of *rab-3*. The constructs were purified and sequenced. Young adult hermaphrodite *npr-15(tm12539)* and WT *C. elegans* were transformed by microinjection of plasmids into the gonad as described (80, 81). Briefly, a mixture containing pPD95_77_*Pnpr-15_npr-15* (40 ng/µl) and *Pmyo-3*::mCherry (5 ng/µl) that drives the expression of mCherry to the muscle as a transformation marker was injected into the animals. For the neuronal rescue, a mixture containing pPD95_77_*Prab-3_npr-15* plasmids (40 ng/µl) and *Pmyo-3*::mCherry (5 ng/µl) that drives the expression of mCherry to the pharynx as a transformation marker was injected into the animals. To rescue *npr-15* in ASJ neurons, *Ptrx-1* promoter and *npr-15* were amplified from gDNA. The *npr-15* fragment was cloned downstream of the *Ptrx-1* by in-fusion PCR to obtain *Ptrx-1::npr-15*, which was cloned into pPD95.77 between the PstI and SmaI sites to generate npr-*15(tm12539);Ptrx-1::npr-15*. The ASJ neuron–specific rescue strain *15(tm12539);Ptrx-1::npr-15* was generated by injecting plasmid

pPD95_77_ *Ptrx-1::npr-15* (25 ng/µl) with *Pmyo-2*::mCherry (10 ng/µl) as a co-injection marker into the *npr-15(tm12539)* and WT which were crossed to *npr-15(tm12539)* animals. Primers used in the generation of transgenic animals are shown in Table S7.

Quantification and Statistical Analysis

Statistical analysis was performed with Prism 8 version 8.1.2 (GraphPad). All error bars represent the standard deviation (SD). The two-sample t-test was used when needed, and the data were judged to be statistically significant when $p < 0.05$. In the figures, asterisks (*) denote statistical significance as follows: NS, Not Significant, *, $p < 0.01$, **, $p < 0.001$, ***, $p < 0.0001$, as compared with the appropriate controls. The Kaplan-Meier method was used to calculate the survival fractions, and statistical significance between survival curves was determined using the log-rank test. All experiments were performed at least three times.

ACKNOWLEDGMENTS

This work was fully supported by NIH grants GM0709077 and AI117911 (to A.A.). Most strains used in this study were obtained from the Caenorhabditis Genetics Center (CGC), which is funded by the NIH Office of Research Infrastructure Programs (P40 OD010440) and the National BioResource Project (NBRP) of Japan.

AUTHOR CONTRIBUTIONS

B.O. and A.A. conceived and designed the experiments. B.O. and A.F.B. performed the experiments. B.O. and A.A. analyzed the data and wrote the paper.

DECLARATION OF INTERESTS

The authors declare no competing interests.

References

1. Netea MG, Schlitzer A, Placek K, Joosten LA, Schultze JL. Innate and adaptive immune memory: an evolutionary continuum in the host's response to pathogens. Cell host & microbe. 2019;25(1):13-26.
2. Gourbal B, Pinaud S, Beckers GJM, Van Der Meer JWM, Conrath U, Netea MG. Innate immune memory: An evolutionary perspective. Immunol Rev. 2018;283(1):21-40.
3. Blander JM, Sander LE. Beyond pattern recognition: five immune checkpoints for scaling the microbial threat. Nature Reviews Immunology. 2012;12(3):215-25.

4. Meisel JD, Kim DH. Behavioral avoidance of pathogenic bacteria by *Caenorhabditis elegans*. Trends Immunol. 2014;35(10):465-70.
5. Sarabian C, Curtis V, McMullan R. Evolution of pathogen and parasite avoidance behaviours. The Royal Society; 2018. p. 20170256.
6. Hart BL, Hart LA. How mammals stay healthy in nature: the evolution of behaviours to avoid parasites and pathogens. Philosophical Transactions of the Royal Society B: Biological Sciences. 2018;373(1751):20170205.
7. Kimbrell DA, Beutler B. The evolution and genetics of innate immunity. Nature Reviews Genetics. 2001;2(4):256-67.
8. Flajnik MF, Du Pasquier L. Evolution of innate and adaptive immunity: can we draw a line? Trends in immunology. 2004;25(12):640-4.
9. Levine B, Mizushima N, Virgin HW. Autophagy in immunity and inflammation. Nature. 2011;469(7330):323-35.
10. Netea MG, Domínguez-Andrés J, Barreiro LB, Chavakis T, Divangahi M, Fuchs E, et al. Defining trained immunity and its role in health and disease. Nature Reviews Immunology. 2020;20(6):375-88.
11. Xiao TS. Innate immunity and inflammation. Cellular & molecular immunology. 2017;14(1):1-3.
12. Geremia A, Biancheri P, Allan P, Corazza GR, Di Sabatino A. Innate and adaptive immunity in inflammatory bowel disease. Autoimmunity reviews. 2014;13(1):3-10.
13. Behringer DC, Butler MJ, Shields JD. Avoidance of disease by social lobsters. Nature. 2006;441(7092):421-.
14. Curtis VA. Infection-avoidance behaviour in humans and other animals. Trends in Immunology. 2014;35(10):457-64.
15. Meisel JD, Kim DH. Behavioral avoidance of pathogenic bacteria by *Caenorhabditis elegans*. Trends in immunology. 2014;35(10):465-70.
16. Styer KL, Singh V, Macosko E, Steele SE, Bargmann CI, Aballay A. Innate immunity in *Caenorhabditis elegans* is regulated by neurons expressing NPR-1/GPCR. Science. 2008;322(5900):460-4.
17. Chang HC, Paek J, Kim DH. Natural polymorphisms in *C. elegans* HECW-1 E3 ligase affect pathogen avoidance behaviour. Nature. 2011;480(7378):525-9.
18. Reddy KC, Hunter RC, Bhatla N, Newman DK, Kim DH. *Caenorhabditis elegans* NPR-1–mediated behaviors are suppressed in the presence of mucoid bacteria. Proceedings of the National Academy of Sciences. 2011;108(31):12887-92.
19. Singh J, Aballay A. Microbial colonization activates an immune fight-and-flight response via neuroendocrine signaling. Developmental cell. 2019;49(1):89-99. e4.
20. Sun J, Singh V, Kajino-Sakamoto R, Aballay A. Neuronal GPCR controls innate immunity by regulating noncanonical unfolded protein response genes. Science. 2011;332(6030):729-32.
21. Balla KM, Troemel ER. *Caenorhabditis elegans* as a model for intracellular pathogen infection. Cellular microbiology. 2013;15(8):1313-22.
22. Schulenburg H, Félix M-A. The natural biotic environment of *Caenorhabditis elegans*. Genetics. 2017;206(1):55-86.
23. Sym M, Basson M, Johnson C. A model for Niemann–Pick type C disease in the nematode *Caenorhabditis elegans*. Current Biology. 2000;10(9):527-30.

24. Nagiel A, Andor-Ardó D, Hudspeth A. Specificity of afferent synapses onto plane-polarized hair cells in the posterior lateral line of the zebrafish. Journal of Neuroscience. 2008;28(34):8442-53.
25. Powell JR, Ausubel FM. Models of *Caenorhabditis elegans* infection by bacterial and fungal pathogens. Innate immunity. 2008:403-27.
26. Singh J, Aballay A. Intestinal infection regulates behavior and learning via neuroendocrine signaling. Elife. 2019;8:e50033.
27. Head BP, Olaitan AO, Aballay A. Role of GATA transcription factor ELT-2 and p38 MAPK PMK-1 in recovery from acute *P. aeruginosa* infection in *C. elegans*. Virulence. 2017;8(3):261-74.
28. Kerry S, TeKippe M, Gaddis NC, Aballay A. GATA transcription factor required for immunity to bacterial and fungal pathogens. PLoS One. 2006;1(1):e77.
29. Olaitan AO, Aballay A. Non-proteolytic activity of 19S proteasome subunit RPT-6 regulates GATA transcription during response to infection. PLoS Genet. 2018;14(9):e1007693.
30. Shapira M, Hamlin BJ, Rong J, Chen K, Ronen M, Tan MW. A conserved role for a GATA transcription factor in regulating epithelial innate immune responses. Proc Natl Acad Sci U S A. 2006;103(38):14086-91.
31. Visvikis O, Ihuegbu N, Labed SA, Luhachack LG, Alves AF, Wollenberg AC, et al. Innate host defense requires TFEB-mediated transcription of cytoprotective and antimicrobial genes. Immunity. 2014;40(6):896-909.
32. Filipowicz A, Lalsiamthara J, Aballay A. TRPM channels mediate learned pathogen avoidance following intestinal distention. Elife. 2021;10:e65935.
33. Garigan D, Hsu A-L, Fraser AG, Kamath RS, Ahringer J, Kenyon C. Genetic analysis of tissue aging in *Caenorhabditis elegans*: a role for heat-shock factor and bacterial proliferation. Genetics. 2002;161(3):1101-12.
34. Cao X, Kajino-Sakamoto R, Doss A, Aballay A. Distinct roles of sensory neurons in mediating pathogen avoidance and neuropeptide-dependent immune regulation. Cell reports. 2017;21(6):1442-51.
35. Sellegounder D, Liu Y, Wibisono P, Chen C-H, Leap D, Sun J. Neuronal GPCR NPR-8 regulates *C. elegans* defense against pathogen infection. Science advances. 2019;5(11):eaaw4717.
36. Kumar S, Egan BM, Kocsisova Z, Schneider DL, Murphy JT, Diwan A, et al. Lifespan extension in *C. elegans* caused by bacterial colonization of the intestine and subsequent activation of an innate immune response. Developmental cell. 2019;49(1):100-17. e6.
37. Hong C, Lalsiamthara J, Ren J, Sang Y, Aballay A. Microbial colonization induces histone acetylation critical for inherited gut-germline-neural signaling. PLoS Biology. 2021;19(3):e3001169.
38. Angeles-Albores D, Lee RY, Chan J, Sternberg PW. Tissue enrichment analysis for *C. elegans* genomics. BMC bioinformatics. 2016;17(1):366.
39. Yang W, Dierking K, Schulenburg H. WormExp: a web-based application for a *Caenorhabditis elegans*-specific gene expression enrichment analysis. Bioinformatics. 2016;32(6):943-5.
40. Kim DH, Feinbaum R, Alloing G, Emerson FE, Garsin DA, Inoue H, et al. A conserved p38 MAP kinase pathway in *Caenorhabditis elegans* innate immunity. Science. 2002;297(5581):623-6.

41. Aballay A, Drenkard E, Hilbun LR, Ausubel FM. *Caenorhabditis elegans* innate immune response triggered by *Salmonella enterica* requires intact LPS and is mediated by a MAPK signaling pathway. Curr Biol. 2003;13(1):47-52.
42. Garsin DA, Villanueva JM, Begun J, Kim DH, Sifri CD, Calderwood SB, et al. Long-lived *C. elegans daf-2* mutants are resistant to bacterial pathogens. Science. 2003;300(5627):1921.
43. Hsu AL, Murphy CT, Kenyon C. Regulation of aging and age-related disease by DAF-16 and heat-shock factor. Science. 2003;300(5622):1142-5.
44. Murphy CT, McCarroll SA, Bargmann CI, Fraser A, Kamath RS, Ahringer J, et al. Genes that act downstream of DAF-16 to influence the lifespan of *Caenorhabditis elegans*. Nature. 2003;424(6946):277-83.
45. Huffman DL, Abrami L, Sasik R, Corbeil J, van der Goot FG, Aroian RV. Mitogen-activated protein kinase pathways defend against bacterial pore-forming toxins. Proc Natl Acad Sci U S A. 2004;101(30):10995-1000.
46. Harris TW, Arnaboldi V, Cain S, Chan J, Chen WJ, Cho J, et al. WormBase: a modern Model Organism Information Resource. Nucleic Acids Res. 2020;48(D1):D762-D7.
47. Lee K, Mylonakis E. An intestine-derived neuropeptide controls avoidance behavior in *Caenorhabditis elegans*. Cell reports. 2017;20(10):2501-12.
48. Furness SG, Sexton PM. Coding GPCR-G protein specificity. Cell Res. 2017;27(10):1193-4.
49. Alcedo J, Kenyon C. Regulation of *C. elegans* longevity by specific gustatory and olfactory neurons. Neuron. 2004;41(1):45-55.
50. Bargmann CI, Horvitz HR. Control of larval development by chemosensory neurons in *Caenorhabditis elegans*. Science. 1991;251(4998):1243-6.
51. Chung SH, Schmalz A, Ruiz RC, Gabel CV, Mazur E. Femtosecond laser ablation reveals antagonistic sensory and neuroendocrine signaling that underlie *C. elegans* behavior and development. Cell reports. 2013;4(2):316-26.
52. Ward A, Liu J, Feng Z, Xu XS. Light-sensitive neurons and channels mediate phototaxis in *C. elegans*. Nature neuroscience. 2008;11(8):916-22.
53. Macosko EZ, Pokala N, Feinberg EH, Chalasani SH, Butcher RA, Clardy J, et al. A hub-and-spoke circuit drives pheromone attraction and social behaviour in *C. elegans*. Nature. 2009;458(7242):1171-5.
54. Frooninckx L, Van Rompay L, Temmerman L, Van Sinay E, Beets I, Janssen T, et al. Neuropeptide GPCRs in *C. elegans*. Frontiers in endocrinology. 2012;3:167.
55. Gupta A, Singh V. GPCR signaling in *C. elegans* and its implications in immune response. Advances in Immunology. 2017;136:203-26.
56. Foster KJ, Cheesman HK, Liu P, Peterson ND, Anderson SM, Pukkila-Worley R. Innate Immunity in the *C. elegans* Intestine Is Programmed by a Neuronal Regulator of AWC Olfactory Neuron Development. Cell Rep. 2020;31(1):107478.
57. Cao X, Aballay A. Neural inhibition of dopaminergic signaling enhances immunity in a cell-non-autonomous manner. Current Biology. 2016;26(17):2329-34.
58. Yu Y, Zhi L, Wu Q, Jing L, Wang D. NPR-9 regulates the innate immune response in *Caenorhabditis elegans* by antagonizing the activity of AIB interneurons. Cellular & molecular immunology. 2018;15(1):27-37.

59. Anderson A, Chew YL, Schafer W, McMullan R. Identification of a conserved, orphan G protein-coupled receptor required for efficient pathogen clearance in *Caenorhabditis elegans*. Infection and immunity. 2019;87(4):e00034-19.
60. Martin N, Singh J, Aballay A. Natural genetic variation in the *Caenorhabditis elegans* response to *Pseudomonas aeruginosa*. G3: Genes, Genomes, Genetics. 2017;7(4):1137-47.
61. Otarigho B, Aballay A. Immunity-longevity tradeoff neurally controlled by GABAergic transcription factor PITX1/UNC-30. Cell reports. 2021;35(8):109187.
62. Ganeshan K, Chawla A. Metabolic regulation of immune responses. Annual review of immunology. 2014;32:609-34.
63. Ganeshan K, Nikkanen J, Man K, Leong YA, Sogawa Y, Maschek JA, et al. Energetic trade-offs and hypometabolic states promote disease tolerance. Cell. 2019;177(2):399-413. e12.
64. Brenner S. The genetics of *Caenorhabditis elegans.* Genetics. 1974;77(1):71-94.
65. Tan MW, Mahajan-Miklos S, Ausubel FM. Killing of *Caenorhabditis elegans* by *Pseudomonas aeruginosa* used to model mammalian bacterial pathogenesis. Proc Natl Acad Sci U S A. 1999;96(2):715-20.
66. Tan MW, Rahme LG, Sternberg JA, Tompkins RG, Ausubel FM. *Pseudomonas aeruginosa* killing of *Caenorhabditis elegans* used to identify *P. aeruginosa* virulence factors. Proc Natl Acad Sci U S A. 1999;96(5):2408-13.
67. Wray C, Sojka WJ. Experimental *Salmonella typhimurium* infection in calves. Res Vet Sci. 1978;25(2):139-43.
68. Sifri CD, Begun J, Ausubel FM, Calderwood SB. *Caenorhabditis elegans* as a model host for *Staphylococcus aureus* pathogenesis. Infect Immun. 2003;71(4):2208-17.
69. Brenner S. The genetics of *Caenorhabditis elegans*. Genetics. 1974;77(1):71-94.
70. Fraser AG, Kamath RS, Zipperlen P, Martinez-Campos M, Sohrmann M, Ahringer J. Functional genomic analysis of *C. elegans* chromosome I by systematic RNA interference. Nature. 2000;408(6810):325-30.
71. Timmons L, Fire A. Specific interference by ingested dsRNA. Nature. 1998;395(6705):854-.
72. Berman JR, Kenyon C. Germ-cell loss extends *C. elegans* life span through regulation of DAF-16 by *kri-1* and lipophilic-hormone signaling. Cell. 2006;124(5):1055-68.
73. Otarigho B, Aballay A. Cholesterol regulates innate immunity via nuclear hormone receptor NHR-8. Iscience. 2020;23(5):101068.
74. Zhu F-Y, Chen M-X, Ye N-H, Qiao W-M, Gao B, Law W-K, et al. Comparative performance of the BGISEQ-500 and Illumina HiSeq4000 sequencing platforms for transcriptome analysis in plants. Plant methods. 2018;14:1-14.
75. Yao L, Wang J, Li B, Meng Y, Ma X, Si E, et al. Transcriptome sequencing and comparative analysis of differentially-expressed isoforms in the roots of *Halogeton glomeratus* under salt stress. Gene. 2018;646:159-68.
76. Jalili V, Afgan E, Gu Q, Clements D, Blankenberg D, Goecks J, et al. The Galaxy platform for accessible, reproducible and collaborative biomedical analyses: 2020 update. Nucleic acids research. 2020;48(W1):W395-W402.
77. Dennis G, Sherman BT, Hosack DA, Yang J, Gao W, Lane HC, et al. DAVID: database for annotation, visualization, and integrated discovery. Genome biology. 2003;4(9):1-11.
78. Heberle H, Meirelles GV, da Silva FR, Telles GP, Minghim R. InteractiVenn: a web-based tool for the analysis of sets through Venn diagrams. BMC bioinformatics. 2015;16:1-7.

79. White JG, Southgate E, Thomson JN, Brenner S. The structure of the nervous system of the nematode *Caenorhabditis elegans.* Philos Trans R Soc Lond B Biol Sci. 1986;314(1165):1-340.
80. Mello CC, Kramer JM, Stinchcomb D, Ambros V. Efficient gene transfer in *C. elegans*: extrachromosomal maintenance and integration of transforming sequences. The EMBO journal. 1991;10(12):3959-70.
81. Mello C, Fire A. DNA transformation. Methods in cell biology. 1995;48:451-82.

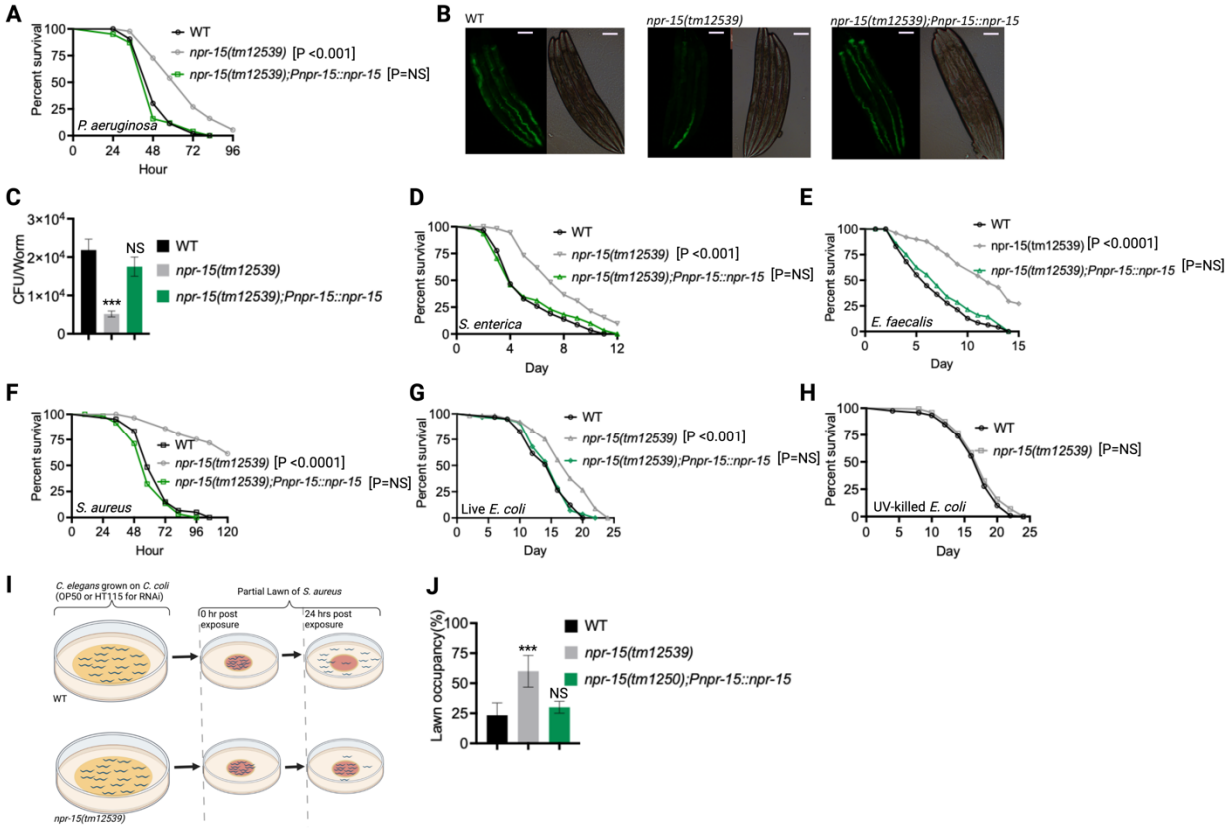

Figure 1. NPR-15 loss-of-function enhanced pathogen resistance and inhibited avoidance behavior.

A. Wild type (WT), *npr-15(tm12539)*, and *npr-15(tm12539);Pnp-15::npr-15* animals were exposed to *P. aeruginosa* partial lawn and scored for survival.
B. Colonization of WT, *npr-15(tm12539)*, and *npr-15(tm12539);Pnp-15::npr-15* animals by *P. aeruginosa*-GFP after 24 hours at 25°C. Scale bar, 200 µm.
C. Colony-forming units per animal [WT, *npr-15(tm12539)*, *npr-15(tm12539);Pnp-15::npr-15*] grown on *P. aeruginosa*-GFP for 24 hours at 25°C. Bars represent means while error bars indicate the SD of three independent experiments; ***$p < 0.001$ and NS = Not Significant.
D. WT, *npr-15(tm12539)*, and *npr-15(tm12539);Pnp-15::npr-15* animals were exposed to *S. enterica* partial lawn and scored for survival.
E. WT, *npr-15(tm12539)*, and *npr-15(tm12539);Pnp-15::npr-15* animals were exposed to *E. faecalis* partial lawn and scored for survival.
F. WT, *npr-15(tm12539)*, and *npr-15(tm12539);Pnp-15::npr-15* animals were exposed to *S. aureus* partial lawn and scored for survival.
G. WT, *npr-15(tm12539)*, and *npr-15(tm12539);Pnp-15::npr-15* animals were exposed to live *E. coli* and scored for survival.
H. WT and *npr-15(tm12539)* animals were exposed to UV-killed *E. coli* and scored for survival.
I. Schematics of avoidance behavior assay on *S. aureus.*

J. Lawn occupancy of WT *C. elegans* and *npr-15(tm12539)*, and *npr-15(tm1250);Pnpr-15::npr-15* animals on a partial lawn of *S. aureus* at 24 hours. Bars represent means while error bars indicate SD; **p < 0.001 and NS = Not Significant.

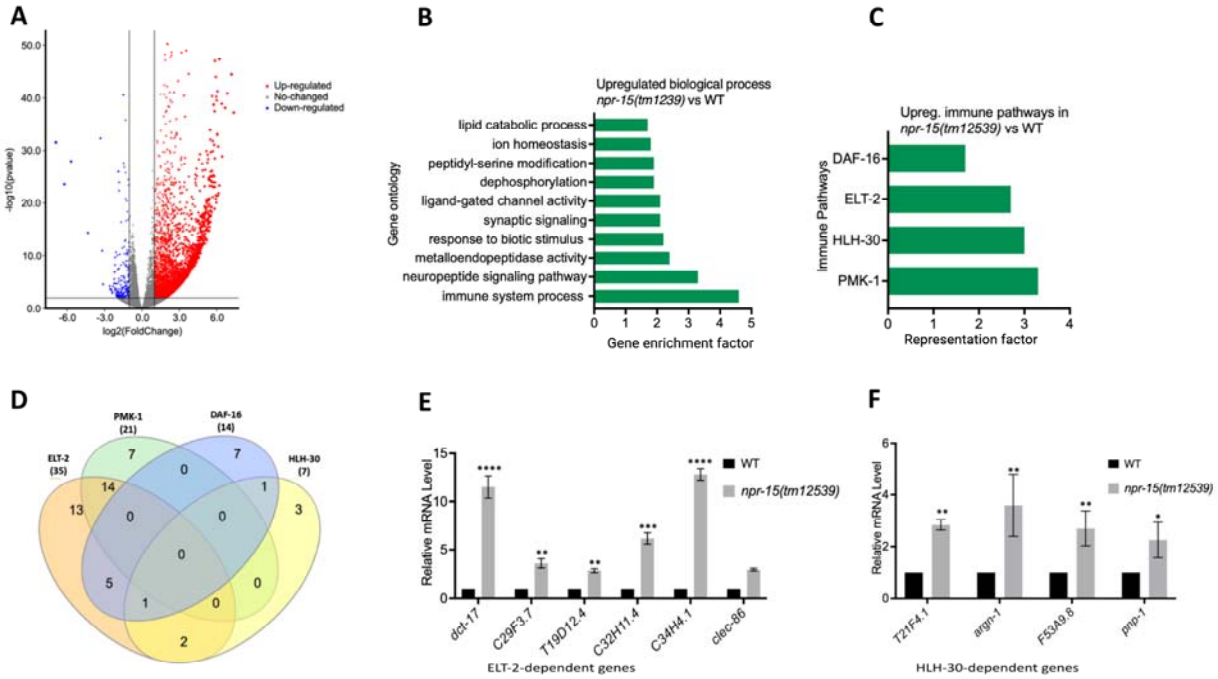

Figure 2. NPR-15 inhibits the expression of immune and aversion-related genes/pathways.

A. Volcano plot of upregulated and downregulated genes in *npr-15(tm12539)* vs. WT animals. Red and blue dots represent significant upregulated and downregulated genes respectively, while the grey dots represent not significant genes.
B. Gene ontology analysis of upregulated genes in *npr-15(tm12539)* vs. WT animals. The result was filtered based on significantly enriched terms, with a Q value < 0.1.
C. Representation factors of immune pathways for the upregulated immune genes in *npr-15(tm12539)* vs. WT animals.
D. Venn diagram showing the upregulated immune genes in each pathway in *npr-15(tm12539)* vs. WT animals.
E. qRT-PCR analysis of ELT-2-depenent immune gene expression in WT and *npr-15(tm12539)* animals. Bars represent means while error bars indicate SD of three independent experiments; *p < 0.05, **p < 0.001, and ***p < 0.0001.
F. qRT-PCR analysis of HLH-30-depenent immune gene expression in WT and *npr-15(tm12539)* animals. Bars represent means while error bars indicate SD of three independent experiments; *p < 0.05, **p < 0.001, and ***p < 0.0001.

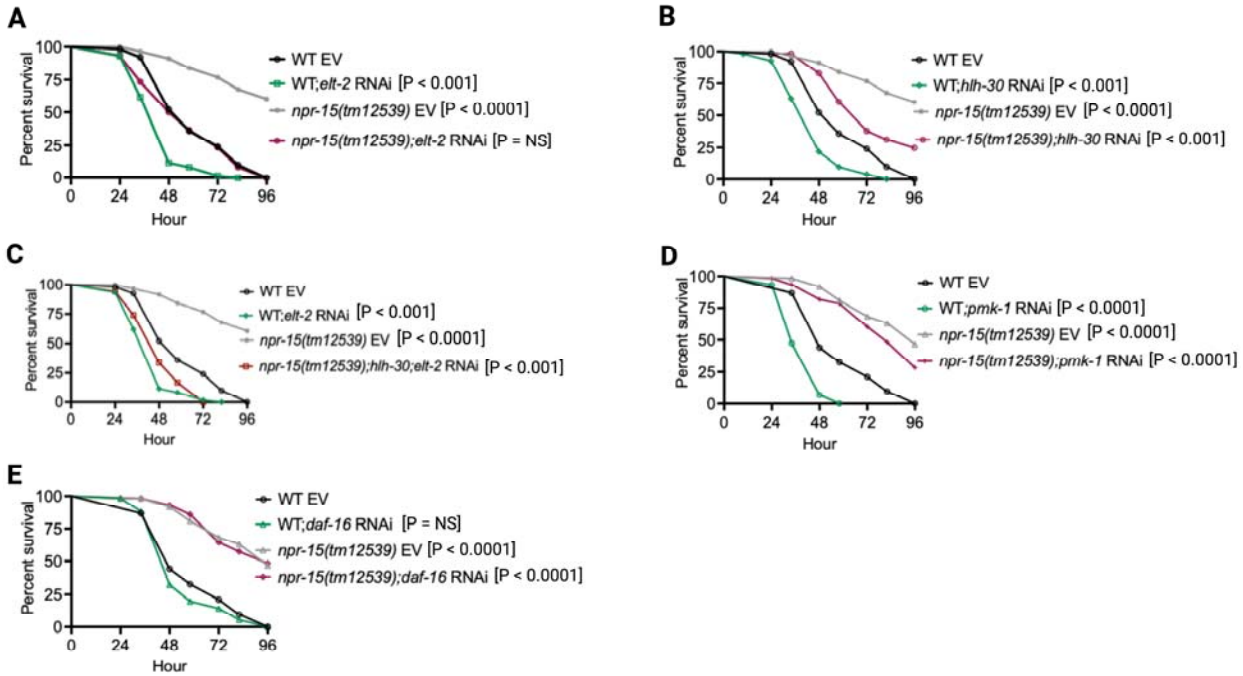

Figure 3: NPR-15 loss-of-function enhances immunity via ELT-2 and HLH-30 when exposed to *S. aureus*.

A. WT and *npr-15(tm12539)* animals fed with *elt-2* RNAi were exposed to *S. aureus* full lawn and scored for survival. EV, empty vector RNAi control.
B. WT and *npr-15(tm12539)* animals fed with *hlh-30* RNAi were exposed to *S. aureus* full lawn and scored for survival. EV, empty vector RNAi control.
C. WT and *npr-15(tm12539)* animals fed with *hlh-30* and *elt-2* RNAi were exposed to *S. aureus* full lawn and scored for survival. EV, empty vector RNAi control.
D. WT and *npr-15(tm12539)* animals fed with *pmk-1* RNAi and animals were exposed to *S. aureus* full lawn and scored for survival. EV, empty vector RNAi control.
E. WT and *npr-15(tm12539)* animals fed with *daf-16* RNAi were exposed to *S. aureus* full lawn and scored for survival. EV, empty vector RNAi control.

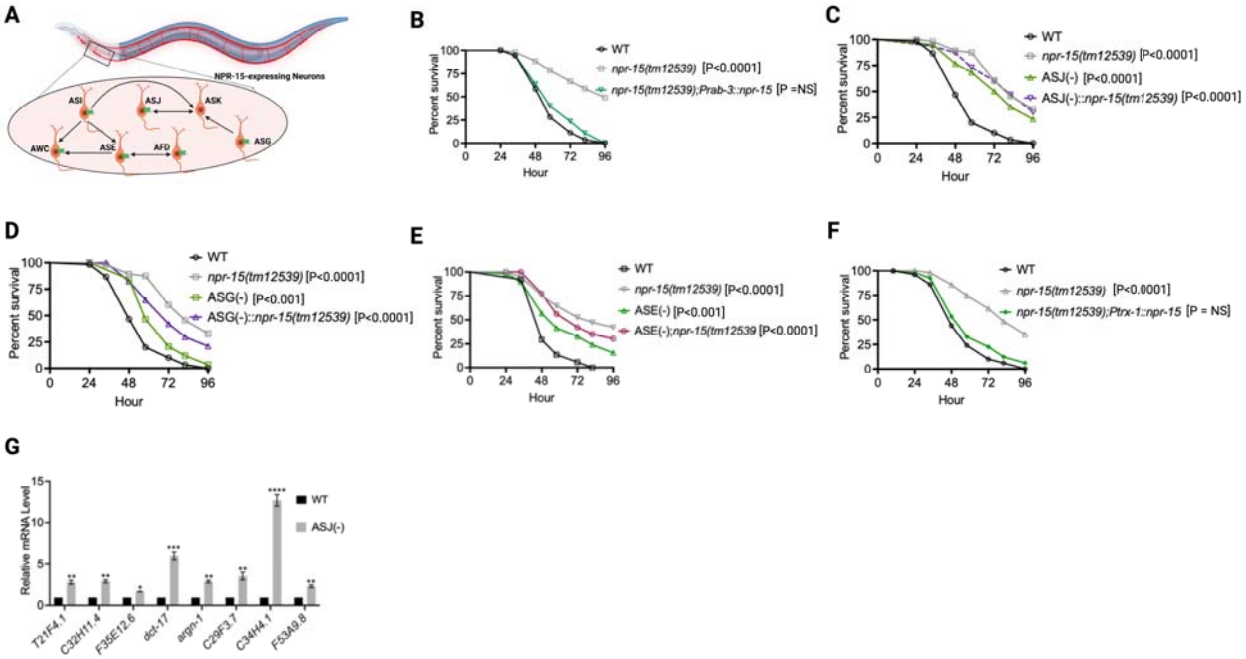

Figure 4. NPR-15 suppresses molecular immune response via sensory neurons, ASJ.

A. Neuronal connectome of NPR-15-expressing neurons.
B. WT, *npr-15(tm12539)*, and *npr-15(tm12539);Prab-3::npr-15* animals were exposed to *S. aureus* full lawn and scored for survival.
C. WT, *npr-15(tm12539)*, ASJ(-), and ASJ(-);*npr-15(tm12539)* animals were exposed to *S. aureus* full lawn and scored for survival.
D. WT, *npr-15(tm12539)*, ASG(-), and ASG(-);*npr-15(tm12539)* animals were exposed to *S. aureus* full lawn and scored for survival.
E. WT, *npr-15(tm12539)*, ASE(-), and ASE(-);*npr-15(tm12539)* animals were exposed to *S. aureus* full lawn and scored for survival.
F. WT, *npr-15(tm12539)*, *npr-15(tm12539);Ptrx-1::npr-15* animals were exposed to *S. aureus* full lawn and scored for survival.
G. qRT-PCR analysis of ELT-2 and HLH-30-depenent immune gene expression in WT and ASJ(-) animals. Bars represent means while error bars indicate SD of three independent experiments; *$p < 0.05$, **$p < 0.001$ and ***$p < 0.0001$.

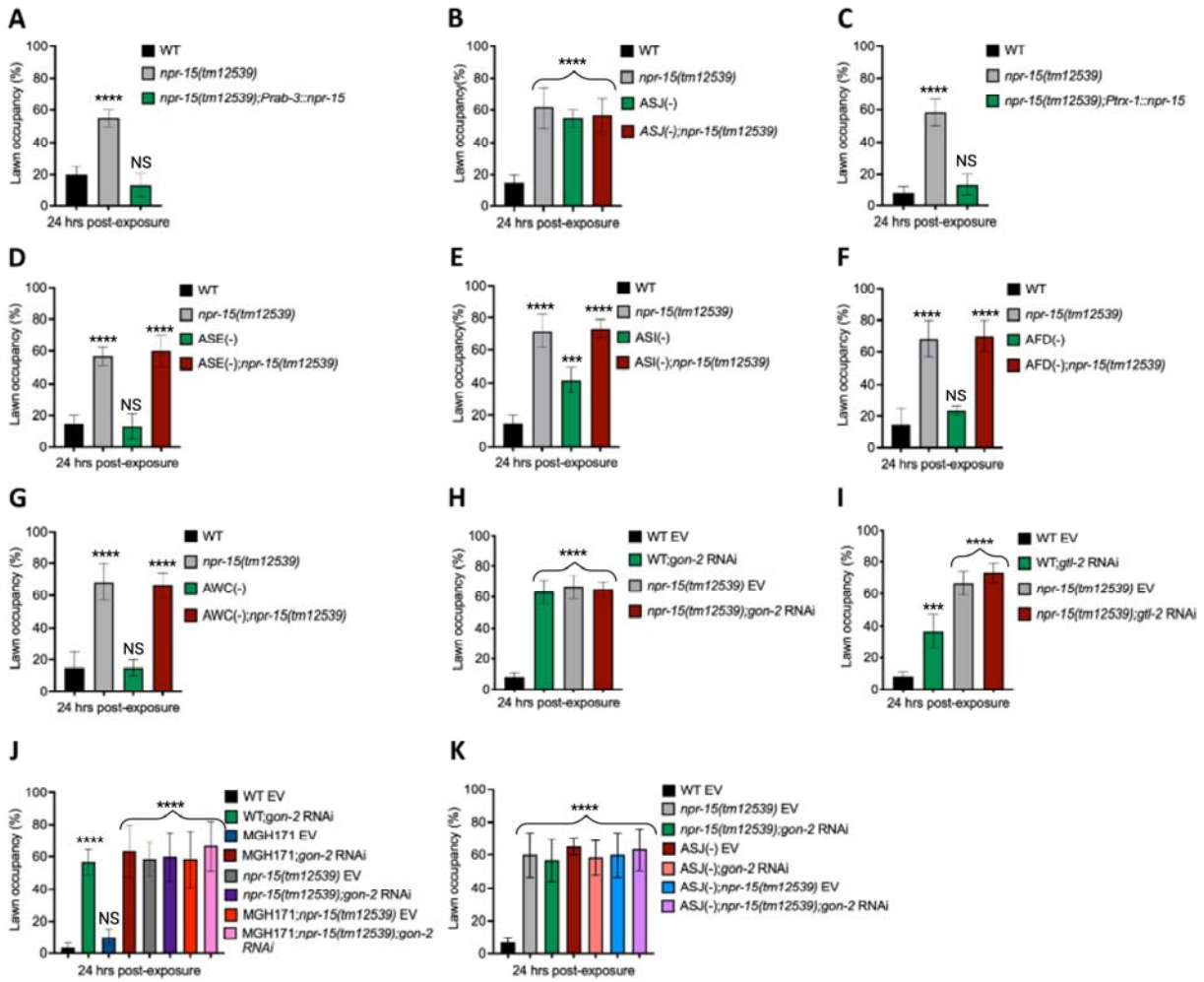

Figure 5: NPR-15 loss-of-function inhibits pathogen avoidance behavior in an ASJ-dependent manner.

- **A.** WT, *npr-15(tm12539)*, and *npr-15(tm12539);Prab-3::npr-15* animals were exposed to partial lawn of *S. aureus* and scored for lawn occupancy. Bars represent means while error bars indicate the SD of three independent experiments; ***p < 0.0001 and NS = Not Significant.
- **B.** WT, *npr-15(tm12539)*, ASJ(-), and ASJ(-);*npr-15(tm12539)* animals were exposed to partial lawn of *S. aureus* and scored for lawn occupancy. Bars represent means while error bars indicate the SD of three independent experiments; ***p < 0.0001 and NS = Not Significant.
- **C.** WT, *npr-15(tm12539)*, and *npr-15(tm12539);Ptrx-1::npr-15* animals were exposed to partial lawn of *S. aureus* and scored for lawn occupancy. Bars represent means while error bars indicate the SD of three independent experiments; ***p < 0.0001 and NS = Not Significant.
- **D.** WT, *npr-15(tm12539)*, ASE(-), and ASE(-);*npr-15(tm12539)* animals were exposed to partial lawn of *S. aureus* and scored for lawn occupancy. Bars represent means while error bars indicate the SD of three independent experiments; ***p < 0.0001 and NS = Not Significant.

E. WT, *npr-15(tm12539),* ASI(-), and ASI(-);*npr-15(tm12539)* animals were exposed to partial lawn of *S. aureus* and scored for lawn occupancy. Bars represent means while error bars indicate the SD of three independent experiments; **p < 0.001, ***p < 0.0001, and NS = Not Significant.

F. WT, *npr-15(tm12539),* and AFD(-), and AFD(-)*;npr-15(tm12539)* animals were exposed to partial lawn of *S. aureus* and scored for lawn occupancy. Bars represent means while error bars indicate the SD of three independent experiments; ***p < 0.0001 and NS = Not Significant.

G. WT, *npr-15(tm12539),* and AWC(-), and AWC(-)*;npr-14(tm12539)* animals were exposed to partial lawn of *S. aureus* and scored for lawn occupancy. Bars represent means while error bars indicate the SD of three independent experiments; ***p < 0.0001 and NS = Not Significant.

H. WT and *npr-15(tm12539)* fed with *gon-2* RNAi and were exposed to the partial lawn of *S. aureus* and scored for lawn occupancy. EV, empty vector RNAi control. Bars represent means while error bars indicate the SD of three independent experiments; ***p < 0.0001.

I. WT and *npr-15(tm12539)* fed with *gtl-2* RNAi and were exposed to the partial lawn of *S. aureus* and scored for lawn occupancy. EV, empty vector RNAi control. Bars represent means while error bars indicate the SD of three independent experiments; **p < 0.001, ***p < 0.0001, and NS = Not Significant.

J. WT, *npr-15(tm12539),* RNAi intestine-specific strain MGH171, MGH171; *npr-15(tm12539)* fed with *gon-2* RNAi and were exposed to the partial lawn of *S. aureus* and scored for lawn occupancy. EV, empty vector RNAi control. Bars represent means while error bars indicate the SD of three independent experiments; ***p < 0.0001 and NS = Not Significant.

K. WT, *npr-15(tm12539),* ASJ(-), ASJ(-);*npr-15(tm12539)* fed with *gon-2* RNAi and were exposed to the partial lawn of *S. aureus* and scored for lawn occupancy. EV, empty vector RNAi control. Bars represent means while error bars indicate the SD of three independent experiments; ***p < 0.0001.

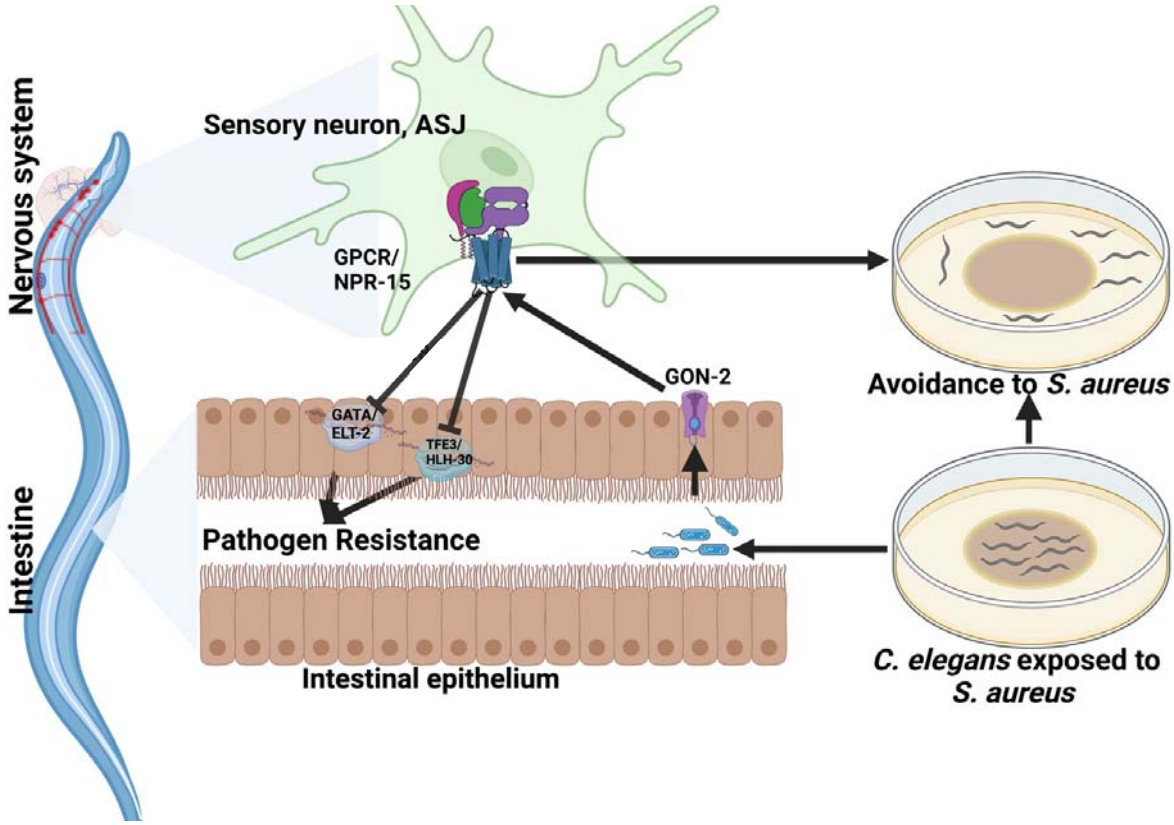

Figure 6: GPCR/NPR-15 suppressed immune response and enhanced avoidance behavior via sensory neurons, ASJ. The immune response control is dependent on ELT-2 and HLH-30 transcription factors. While NPR-15 controls avoidance behavior to *S. aureus* via intestinal-expressed TRPM channel, GON-2.